OXFORD

ORIGINAL ARTICLE

Apoptotic Markers in the Midbrain of the Human Neonate After Perinatal Hypoxic/Ischemic Injury

Marianna A. Pagida, PhD, Anastasia E. Konstantinidou, MD, PhD,
Margarita A. Chrysanthou-Piterou, PhD, Efstratios S. Patsouris, MD, PhD, and
Maria T. Panayotacopoulou, PhD

Abstract

Our previous postmortem studies on neonates with neuropathological injury of perinatal hypoxia/ischemia (PHI) showed a dramatic reduction of tyrosine hydroxylase expression (dopamine synthesis enzyme) in substantia nigra (SN) neurons, with reduction of their cellular size. In order to investigate if the above observations represent an early stage of SN degeneration, we immunohistochemically studied the expression of cleaved caspase-3 (CCP3), apoptosis inducing factor (AIF), and DNA fragmentation by using terminal deoxynucleotidyltransferase-mediated dUTP-biotin 3′-end-labeling (TUNEL) technique in the SN of 22 autopsied neonates (corrected age ranging from 34 to 46.5 gestational weeks), in relation to the severity/duration of PHI injury, as estimated by neuropathological criteria. No CCP3-immunoreactive neurons and a limited number of apoptotic TUNEL-positive neurons with pyknotic characteristics were found in the SN. Nuclear AIF staining was revealed only in few SN neurons, indicating the presence of early signs of AIF-mediated degeneration. By contrast, motor neurons of the oculomotor nucleus showed higher cytoplasmic AIF expression and nuclear translocation, possibly attributed to the combined effect of developmental processes and increased oxidative stress induced by antemortem and postmortem factors. Our study indicates the activation of AIF, but not CCP3, in the SN and oculomotor nucleus of the human neonate in the developmentally critical perinatal period.

Key Words: Apoptosis inducing factor (AIF), Cleaved caspase-3 (CCP3), DNA fragmentation, Human substantia nigra, Oculomotor nucleus, Perinatal hypoxia/ischemia, Perinatal infection.

INTRODUCTION

Perinatal hypoxia/ischemia (PHI)—a major underlying mechanism for most obstetric complications in humans—remains a most commonly reported mode of perinatal death globally. Despite the improvement in intensive care unit technology during the last years, every year, ∼0.5 million infants that survive from PHI develop motor, sensory and/or cognitive impairments (for review, [1]). Epidemiological studies have shown that PHI is a potential risk factor for the development of neurological and psychiatric disorders later in life, including cerebral palsy, mental retardation, learning and memory disabilities, developmental forms of Parkinsonism, schizophrenia, and attention deficit hyperactivity disorder (ADHD) (2–6).

The substantia nigra (SN) and the ventral tegmental area, located in the midbrain, contain the majority of the dopaminergic neurons in the brain and are involved in motor control, cognitive, and rewarding behaviors (7, 8). Dysregulation of dopaminergic neurotransmission underlies the pathophysiology of many neurological and neuropsychiatric disorders, notably Parkinson disease (9), schizophrenia (10, 11), and ADHD (12). Experimental studies indicate that SN neurons are especially vulnerable to PHI by causing long-term changes in the number of tyrosine hydroxylase (TH; first and rate limiting enzyme in dopamine synthesis)-immunoreactive (IR) neurons (13–16). In rats, unilateral carotid ligation at postnatal day 7 (the age corresponding to that of the full-term human neonate), results in decreased number of SN neurons in the adulthood (14). This decrease in dopaminergic neurons has been associated with an increase in apoptotic cell death events in SN following early striatal injury caused by PHI, as indicated by silver staining and in situ 3′-end-labeling of DNA (17). Umbilical cord occlusion at late-gestation in pregnant sheep causes a significant increase of cleaved caspase-3 (CCP3; apoptotic marker)-IR cells in many vulnerable areas of the offspring's brains, including SN, despite the fact that cells in SN do not present any pyknotic features with routine hematoxylin and eosin staining (18).

Despite the difficulties in dissociating the contribution of other insults (e.g. acidosis, infection, or genetic causes) to the induction of the perinatal neuropathological injury, we have previously shown a dramatic reduction or even absence of TH expression in the SN neurons of human neonates with neuropathological injury of prolonged/older or chronic

PHI ([19](19)). Interestingly, most of the SN neurons in our sample were significantly smaller, without any evidence of pyknosis. The question raised, therefore, was whether this significant decrease in both size and ability to synthesize dopamine reflects an early stage of degeneration in the SN neurons of the human neonate after PHI events.

The purpose of the present study was to investigate the possible activation of apoptotic mechanisms in SN neurons of human neonates showing different severity/duration of the neuropathological PHI injury. We focused on (i) CCP3, the main effector protein of classical apoptosis, playing a central role in the initiation and regulation of the proteolytic events leading to cell death ([20](20)). CCP3 is widely used as a marker for detecting neurons in the early stages of apoptosis, even before neurons display the typical morphological characteristics of apoptosis, such as chromatin degradation. (ii) DNA fragmentation, a typical morphological characteristic of apoptotic neurons, using the in situ terminal deoxynucleotidyltransferase-mediated dUTP-biotin 3′-end-labeling (TUNEL) method ([21–23](21)). (iii) Apoptosis inducing factor (AIF) that normally promotes cell survival when it resides in the mitochondria, but activates a caspase-independent apoptotic-like death program when it translocates to the nucleus (for review, [[24](24)]).

MATERIALS AND METHODS

Patients and Tissues

Formalin-fixed midbrains of 22 autopsied neonates (11 male and 11 female) were obtained from the Greek Brain Bank (GBB; member of Brain-Net Europe) in accordance with the Declaration of Helsinki and approved by the ethics committee of School of Health Sciences (National and Kapodistrian University of Athens). Part of this material was also used in our previous studies ([19, 25](19)). Complete postmortem examination was carried out in all cases after parental written consent for diagnostic and research purposes.

The corrected age of the neonates (duration of pregnancy + postnatal age) ranged from 25.5 to 46.5 weeks ([Table 1](table1)). Nine infants (5 male and 4 female) were delivered by emergency cesarean section. Five infants (1 male and 4 female) were prematurely born before week 36 of gestation, while the remaining neonates were delivered at or near term. The majority of subjects were born alive, except cases GBB 3143/12, 170/16, 274/17, 3340/15, 311/18, 2631/09, and 3161/13 who were fresh stillbirths or intrapartum deaths. Late intrauterine fetal deaths were excluded to avoid brain autolysis.

In order to evaluate the expression of the above apoptotic markers also in the human adult control and degenerating SN, we included in our sample sections from the midbrain of 2 control adults (BM2, B28) and 1 Parkinsonian patient (2451), respectively ([Table 1](table1)), obtained from the archival M. Issidorides brain tissue collection of Eginition Hospital, University of Athens.

Histopathology

The neuropathological evaluation of PHI injury was based on established criteria dependent on the pattern of gray and/or white matter lesions (included in the spectrum of neuronal necrosis and periventricular leukomalacia changes) in specific brain regions ([26–28](26)), summarized in [Table 2](table2) and described in details in our previous work ([19, 29](19)). Three neuropathological groups of PHI were used: group 1, severe/acute PHI injury; group 2, moderate/prolonged or older injury; and group 3, very severe/long duration, old, or chronic PHI injury. When multiple lesions coexisted (combinations of gray and white matter injury or multiple lesions of varying severity/onset of duration), the highest score observed was assigned to the case. Clinical and pathological data as well as the neuropathological PHI grading of the subjects studied are presented in [Table 1](table1).

In view of the limitation of working with human autopsy samples and considering that all autopsied neonates who fulfilled the criteria of inclusion sustained some degree of hypoxic insult, true "controls" were difficult to include in this study. In our sample, only 2 subjects GBB 170/16 and GBB 274/17, stillborn neonates with signs of acute asphyxia, but no evidence of neuropathological injury in specific brain areas ([Table 2](table2)), were used as "controls."

Histology and Immunohistochemistry

The midbrains were dehydrated in graded alcohol and embedded in paraffin blocks that were serially cut in 7-μm-thick sections. One section for every 100 from the rostrocaudal extent of the midbrain was mounted on silane-coated slides and stained with Cresyl violet/Luxol fast blue, as previously described ([19](19)), to define the different anatomical levels of the midbrain (based on [[30](30)]). The level of the red and oculomotor nucleus, where the fibers of the third nerve first appear (see Fig. 56 from brainstem atlas [[30](30)]), was chosen for 2 reasons: first, SN neurons are clearly separated from other dopaminergic groups, that is, paranigral and parabrachial nucleus, due to the anatomical borders made by the third nerve fibers; second, this level of the midbrain was used in our previous work for the study of TH-IR neurons in SN ([19](19)). Five consecutive sections were stained, respectively, for (i) hematoxylin and eosin (H&E) for routine histological evaluation ([29](29)); (ii and iii) CCP3 with 2 different polyclonal antibodies (Asp175, #9661, Cell Signaling Technology, The Netherlands and #559565, clone C92-605, BD Biosciences, San Jose, CA, respectively) that both recognize the active form of caspase-3 in human and mouse cells (especially the large fragment 17, 19 or 20 kDa) and not the proenzyme form of caspase-3 or other cleaved caspases; (iv) TUNEL (S7100, ApopTag Peroxidase In Situ Apoptosis Detection Kit, Merck, Darmstadt, Germany); and (v) AIF (AB16501, Merck). Sections from all cases studied were simultaneously processed for each histological/immunohistochemical procedure.

For the detection of CCP3 from Cell Signaling Technology, sections were deparaffinized in xylene ($2\times$ 10 minutes), rinsed in 100% ($2\times$ 5 minutes), 95%, 85%, and 75% ethanol for 5 minutes each, and then washed in distilled water (dH$_2$O) ($2\times$ 5 minutes). Sections were proceeded for antigen retrieval procedure with citrate buffer (10 mM citric acid monohydrate, #100244, Merck, pH = 6.0) using microwaves at 400 W ($2\times$ 5 minutes). Sections were cooled at room temperature (RT), washed in dH$_2$O and in Tris-buffered saline (TBS; 0.05 M

TABLE 1. Clinical and Pathological Data of Cases Studied and Neuropathological Perinatal Hypoxic/Ischemic (PHI) Groups

GBB No.	Age (w, d, h) (Total Age, w) Sex	Postmortem Delay (Days)/*Fixation Time (Months)*	Body Weight (g)/*Percentile*	Brain Weight (g)	Head Perimeter (cm)/*Percentile*	Clinical and Pathological Data*/*Medications*	PHI Group
3143/12	25.5w + 0h (25.5w) M	2/*9.8*	811/*53th*	121	24.0/*50*	Stillborn: chondrodysplasia punctata/(–)	1
2426/08	32.5w + 3h (32.5w) F	4/*2.5*	2032/*38th*	219	31.0/*90*	Neonatal pneumonia, persistent fetal circulation, cholestasis	2
2226/07	27w + 52d (34w) F	<1/*2.5*	1370/*1st*	198	ND	RDS, BPD, septicemia, renal failure/*surfactant, antibiotics, inotropes, diuretics, sedatives, TPN*	3
170/16	35w + 0h (35w) F	*2/12*	*3493/86th*	348	34.7/*97*	Stillborn: maternal diabetes, acute hypoxia, hypertrophic cardiomyopathy, chorionic villous immaturity	0
274/17	36w + 0h (36w) F	*2/4.7*	*2148/5th*	340	31.5/*10–50*	Stillborn: SGA—chorionic villous immaturity	0
1139/03	34w + 21d (37w) M	3/*8*	2880/*31st*	275	28.5/*<3*	Down syndrome, congenital cyanotic heart defect, hypotension and bradycardia episodes/*antibiotics, inotropes, TPN*	3
2807/07	37w + 0h (37w) M	2/*2.5*	2445/*7th*	444	32.5/*25–30*	Acute thrombosis of the umbilical vein	1
3415/16	37.5w + 0.5h (37.5w) F	2/*23*	*3213/57th*	416	34.5/*50–90*	Chondroectodermal dysplasia (Ellis van Creveld): pulmonary hypoplasia—cardiac defects—skeletal dysplasia	1
2631/09	38w + 0h (38w) F	<0.5/*3*	3970/*94th*	392	36.5/*90–97*	Stillborn infant of diabetic mother—macrosomia, cardiomyopathy, organomegaly, pancreatic islet hyperplasia	1
237/17	39w + 2d (39w) M	*1/2*	3030/*20th*	367	34.5/*50*	Intrauterine pneumonitis—congenital ventriculomegaly	2
1965/06	39w + 2h (39w) M	2/*1*	2744/*7th*	337	34.0/*50*	Congenital cyanotic heart defect, dyspnea, acidosis, heart failure/*inotropes, adrenaline, bicarbonates*	2
2735/09	39w + 2d (39.5w) F	0.3/*6*	2960/*16th*	313	32.0/*3*	Fatty acid oxidation defect—liver steatosis, cardiomyopathy, pancreatic islet hyperplasia—vomiting, hypoglycemia, cardiac arrest	1
1836/06	35w + 29d (39w) M	3/*8*	1950/*1st*	310	31.0/*<3*	Congenital cyanotic heart defect and heterotaxy, apslenia (Ivemark syndrome), dyspnea, arrhythmia, acidosis/*antibiotics, inotropes (adrenaline, bicarbonates), TPN*	2
3340/15	39.5w + 0h (39.5w) F	3/*1.1*	2760/*7th*	416	32/*3*	Stillborn: fetal thrombotic vasculopathy	2
3907/07	39.5w + 2h (39.5w) F	1.5/*1*	3255/*37th*	380	35.0/*50*	Lung atelectasis, acidosis/*adrenaline, bicarbonates*	1
3161/13	40w + 0h (40w) F	1/*1.4*	3100/*19th*	467	34.5/*25–50*	Intrapartum death: umbilical cord prolapse, hypoxic placenta	1
311/18	40w + 0h (40w) M	2/*2*	*3330/33rd*	495	36.8/*90*	Stillborn: fetomaternal hemorrhage	2
1593/05	41w + 1d (41w) M	2/*2*	3120/*19th*	380	33.0/*3–10*	Congenital cyanotic heart defect, congenital viral infection, meconium aspiration/*antibiotics, inotropes, adrenaline*	3
2062/07	28w + 103d (43w) M	0.7/*4*	2280/*1st*	283	30.5/*<3*	Cystic fibrosis, RDS, respiratory infection—irritability, hypotention, hypoxemia, acidosis/*surfactant, antibiotics, inotropes, diuretics, sedatives, TPN*	3

(continued)

TABLE 1. Continued

GBB No.	Age (w, d, h) (Total Age, w) Sex	Postmortem Delay (Days)/*Fixation Time (Months)*	Body Weight (g)/*Percentile*	Brain Weight (g)	Head Perimeter (cm)/*Percentile*	Clinical and Pathological Data*/*Medications*	PHI Group
1402/04	25w + 136d (44w) M	3/*8*	3000/*15th*	300	34.0/*3*	Twin gestation, RDS, renal failure, congenital cystic renal hypodysplasia, endocardial fibroelastosis, myocardial ischemia, brain hemorrhage, seizures, multiorgan failure/*surfactant, antibiotics, corticosteroids, anticonvulsants, inotropes, diuretics, sedatives, TPN*	3
1286/04	35w + 67d (44.5w) M	3/*12*	3800/*25th*	347	34.5/*3*	Placental insufficiency, respiratory infection, cholestasis, adrenal hypoplasia—profound hypotonia, persistent seizures, absence of reflexes, cardiac arrest/*antibiotics, anticonvulsants, sedatives, inotropes (adrenaline), TPN*	3
1163/04	28w + 130d (46.5w) F	4/*0.5*	3100/*<3rd*	105	33.0/*<3*	Sepsis, necrotizing enterocolitis, renal—liver failure—Seizures, multiorgan failure/*surfactant, antibiotics, anticonvulsants, sedatives, inotropes, diuretics, TPN*	3

Adults

No.	Age(Years)/ Sex	Postmortem Delay (Hours)	*Fixation Time (Days)*		
B28	52/F	36	46	Myocardia ischemic infarct	
BM2	67/F	36	18	Aortic aneurysm	
2451	77/F	3	300	Parkinson and Alzheimer disease, atherosclerosis	

GBB, Greek Brain Bank; F, female; M, male; w, weeks of gestation; h or d, hours or days of postnatal life; RDS, respiratory distress syndrome; SGA, small for gestational age; TPN, total parenteral nutrition.
*Excluding neuropathological findings.

TABLE 2. Perinatal Hypoxic/Ischemic (PHI) Injury Groups Based on Neuropathological Criteria

PHI Injury	Severity/Duration/Timing of the Insult		
Gray matter injury	**Severe/abrupt**	**Moderate/prolonged/older**	**Very severe/long duration/old**
Topography of neuronal necrosis	Thalamus	Cerebral cortex	Diffuse neuronal necrosis
	Basal ganglia	Thalamus	Neuronal mineralization
		Basal ganglia	
White matter injury	**Acute**	**Subacute**	**Chronic**
Histopathological findings	Coagulation necrosis	Endothelial hyperplasia	Glial scar
	Axonal swellings	Microglial proliferation	Cavitation
		Microcalcifications	
		Reactive gliosis	
PHI groups	Group 1	Group 2	Group 3

Tris, 0.15 M NaCl, pH = 7.6) and incubated in 5% milk in TBS for 45 minutes. After washing, sections were incubated in 5% normal goat serum (NGS; GO-605, Biosera, Nuaille, France) for 30 minutes and then in the primary CCP3 antiserum (1:350 in 1% NGS) for 1 hour at RT and subsequently, for 2 days at 4°C. After washing, sections were incubated in a secondary polyclonal goat antirabbit biotinylated antibody (1:100, BA-9200, Vector, Burlingame, CA) in TBS for 1 hour at RT. Then, sections were washed in TBS and incubated with avidin-biotin complex (Vectastain ABC KIT, PK-4000, Vector, 1:400) for 1 hour at RT. After washing in TBS and then in 0.1 M Tris-HCl buffer (pH = 7.6) for 15 minutes, sections

were incubated in 0.5 mg/mL 3,3′-diaminobenzidine tetrahydrochloride (DAB) (D5905, Sigma-Aldrich) in Tris-HCl containing 0.02% nickel ammonium sulfate ([Ni] Johnson Matthey Alfa Products, Germany) and 0.01% H_2O_2 (Merck) for a few minutes, washed in tap water, dehydrated, and mounted in DPX (BDH, Poole, United Kingdom).

For the detection of CCP3 from BD Biosciences, dehydrated sections were proceeded for antigen retrieval with Tris-EDTA buffer (10 mM Tris Base, 1 mM EDTA solution, 0.05% Tween 20, pH = 9.0) in microwaves at 400 W (2× 5 minutes). Sections were cooled at RT, washed in dH_2O and TBS, and bathed in 3% H_2O_2 diluted in 50% methanol with TBS for 30 minutes in order to quench the endogenous peroxidase. After washing in TBS, sections were incubated in 10% NGS for 30 minutes and then in the primary CCP3 antiserum (1:500 in 1% NGS) overnight at 4°C. As a positive control for CCP3 staining, a thymus biopsy from a 40-year-old man was used (kindly provided by Dr George Koutlis). Thymus tissue displayed normal parenchyma (as assessed using a light green counterstaining) and contained numerous apoptotic cells, as previously described (31). The specificity of the CCP3 immunohistochemical reaction was checked by omitting the primary antibody from the incubation medium. Although no major differences were revealed in the CCP3 immunoreaction between the 2 antibodies, our results and figures were based on sections stained with the BD Bioscience antibody because of the better quality of the immunohistochemical reaction.

For TUNEL staining, we followed the protocol proposed by the manufacturer. In brief, sections were deparaffinized and immersed to 10 mM phosphate-buffered saline (PBS) (1×). Sections were pretreated with 20 μg/mL proteinase K (A3830, AppliChem, Darmstadt, Germany) for 15 minutes, washed in dH_2O for 2× 2 minutes and remained in 3% H_2O_2 in PBS for 5 minutes at RT. After washing in PBS, slices remained in the equilibration buffer for 7 minutes and were then incubated with the working strength TdT Enzyme for 1 hour in a humidified chamber at 37°C. The reaction was stopped with the application of stop/wash buffer and sections were incubated with antidigoxigenin for 30 minutes. The TUNEL reaction was visualized using DAB-Ni. Sections were lightly counterstained in 0.5% methylene blue (M9140; Sigma-Aldrich, Taufkirchen, Germany) for 10 minutes, then washed in dH_2O and butanol, dehydrated to xylene and coverslip with DPX. In sections used as a negative control, TdT enzyme was omitted by the incubation buffer.

For the detection of AIF, dehydrated sections were proceeded for antigen retrieval procedure with 10 mM citrate buffer (pH = 6.0) in microwave at 400 W (2× 5 minutes). After washing in TBS, slides immersed in 5% milk in TBS for 45 minutes and 10% NGS in TBS for 1 hour and then incubated with the primary polyclonal AIF antibody (1:2500 and 1:2000 for neonatal and adult brain, respectively) for 1 hour at RT and then overnight at 4°C. The reaction was revealed by DAB-Ni. The specificity of the AIF reaction was checked by omitting the primary antibody from the incubation medium.

In order to check the distribution of AIF labeling in neurons showing eosinophilic cytoplasm and pyknosis in H&E

preparations, an extra section of each case was first stained for H&E, photographed, and then destained (with 1% hydrochloric acid in 80% alcohol for 3–4 minutes) and restained for AIF, as described above.

Morphometric and Statistical Analysis in AIF-Stained Sections

The morphometric analysis was independently performed by 2 individuals (MPag and MC-P) in the SN, as well as in the oculomotor nucleus, since this nucleus displayed especially high AIF immunoreactivity (see "Results"). Ten to 15 AIF-stained neurons per case with unlabeled nucleus were unilaterally captured at a magnification of ×400, using a digital charge-coupled device color video-camera (SSC-C370P; Sony, Tokyo, Japan) connected to an optical microscope (BX50F-3; Olympus, Tokyo, Japan). The cytoplasmic optical density (OD) of AIF staining, the cellular and nuclear size were measured using the image analysis software IMAGE-PRO PLUS, version 4.5.1.29 (Media Cybernetics, Bethesda, MD). Five to 10 neurons with a defined nuclear AIF staining were also morphometrically studied only in the oculomotor nucleus.

The percentage of neurons with nuclear AIF staining was estimated by counting all the neurons with nuclear AIF staining out of the total number of AIF-stained neurons (with stained or unstained nucleus) in 10 randomly selected ×200 fields in the SN and oculomotor nucleus.

For the statistical analysis, the nonparametric Spearman rank correlation test was used and performed in SPSS (v. 18.0.0, Chicago, IL), in order to reveal possible correlations between the measured variables with PHI grading, the corrected (gestational and postnatal) age, sex, brain weight, head perimeter, the presence of infection, the postmortem delay, and fixation time. The AIF OD values of case GBB 237/17 were excluded from the statistical analysis, as extreme values. In addition, the nonparametric Wilcoxon test was used to check possible differences between SN and oculomotor neurons. The cases GBB 2226/07, 1139/03, 3907/07, and 2807/07 were not included in the statistical analysis because the oculomotor nucleus was not clearly delineated at the available levels of the midbrain. The means with the standard error of the mean (SEM) were calculated for each variable. $p < 0.05$ was considered statistically significant.

RESULTS

Cleaved Caspase-3
Substantia Nigra

In the midbrain of the human neonate, no CCP3 staining in SN neurons was revealed by immunohistochemistry, independently of the postmortem delay, fixation time, and the severity/duration of PHI injury (Fig. 1A). However, some glial cells positive for CCP3 were sporadically observed within the SN of some cases (Fig. 1B, arrow). GBB 3415/16 was the only neonate in which a limited number of CCP3-positive SN neurons was observed (Fig. 1C). This neonate died within 30 minutes after birth with acute respiratory distress and was diagnosed with a genetic skeletal dysplasia causing severe pulmonary hypoplasia. In neonate GBB 1836/06, with transposi-

tion of great arteries in the context of Ivermark's syndrome, many CCP3-stained glial cells were found in the SN (Fig. 1D, arrows), without any evidence for neuronal CCP3 staining. This large number of CCP3-positive glial cells was not observed in any other case of our sample.

In sections from the thymus biopsy, used as a positive control tissue for CCP3 staining, many apoptotic CCP3-positive leucocytes were evident among normal epithelial cells (Fig. 1E). In addition, many CCP3-labeled apoptotic cells were observed in areas with focal hemorrhages in neonate GBB 1402/04, tissue used as an internal positive control for CCP3 staining (Fig. 1F).

In the 2 adult control subjects, the majority of melanized SN neurons exhibited an intense granular CPP3 staining intermingled with melanin granules in their cytoplasm (Fig. 1G), as also previously reported for adult humans by Hartmann et al (32). In the degenerating SN of the Parkinsonian case, only a few melanized neurons revealed a diffuse, intense CCP3 immunohistochemical reaction in their cytoplasm (Fig. 1H). In the same case, CCP3 reaction was also observed within Lewy bodies (Fig. 1I) and in large round intranuclear inclusions (Fig. 1J), probably corresponding to Marinesco bodies in a few SN neurons. In sections stained by omitting the primary antibody to check the specificity of the immunohistochemical reaction, no staining was evident.

Oculomotor Nucleus

Absence of CCP3 immunohistochemical staining was also revealed in the neurons of the oculomotor nucleus and other midbrain neuronal groups, such as superior colliculi, ventral tegmental area, and raphe nucleus. Only few CCP3-stained glial cells were sporadically encountered in some cases. In neonate GBB 1836/06 (Ivemark syndrome), a large number of CCP3-positive glial cells were revealed not only in the SN, as described above, but also inside the oculomotor nucleus and its fibers.

TUNEL Staining
Substantia Nigra

For the interpretation of the TUNEL results, the positivity (or not) of the nuclear staining and the distribution/density of the labeling combined with the nuclear morphology were taken into consideration. In the "control" neonate GBB 170/16 (case without evidence for neuropathological PHI lesions), no TUNEL-positive nuclei were revealed in SN neurons, while numerous TUNEL-positive glial cells were evident (Fig. 2A). Typical apoptotic nuclear morphology, as depicted by dense, shrunken and intense nuclear TUNEL staining, was observed in only a limited number of TUNEL-positive neurons with pyknotic characteristics within the SN of hypoxic neonates (Fig. 2B, C, see arrows). In the majority of PHI group 1 neonates, a large number of nuclei showed light TUNEL staining that outlined the nucleus and the nucleolus (Fig. 2B). In cases with prolonged/old or chronic PHI, the intensity of the TUNEL staining was significantly increased in SN neurons (compare a case of PHI group 3, Fig. 2C vs a case of group 1, Fig. 2B]). The majority of TUNEL-positive neurons showed a

diffuse, loose distribution of TUNEL-labeled nuclear chromatin (Fig. 2D, long arrows), which is not indicative of the typical apoptotic morphology, that is, chromatin condensation and/or the formation of blebs.

The differential intensity of the nuclear staining among neonates did not seem to result from prolonged postmortem delay. For example, neonates GBB 3161/13 (group 1) and 2226/07 (group 3), both having a short postmortem delay ($\leq$1 day), exhibited substantial differences in the TUNEL labeling levels, the more intense of which were observed in case 2226/07 with neuropathological lesions consistent with prolonged PHI (compare Fig. 2E with Fig. 2F).

In all cases studied, extensive TUNEL staining was always found in glial cells, not only within the SN but also in the whole mesencephalic section. Glial nuclei showed differential pattern of staining with (i) intensely condense nuclear TUNEL staining indicative of the apoptotic morphology (Fig. 2D, thick arrowhead), (ii) diffusely, loose nuclear TUNEL labeling indicative of a non-apoptotic morphology (Fig. 2D, short arrow), and (iii) intense TUNEL positivity in both soma and processes corresponding to necrotic characteristics (Fig. 2D, white arrow). These differential glial TUNEL morphologies were seen in the majority of the cases studied, although their proportion varied among them.

Oculomotor Nucleus

In the "control" neonate GBB 170/16, no TUNEL-positive neurons were revealed in the oculomotor nucleus. In hypoxic neonates, the majority of oculomotor neurons displayed diffuse, loose distribution of TUNEL-labeled nuclear chromatin (non-apoptotic morphology), whereas few TUNEL-positive neurons showed a typical apoptotic nuclear morphology in only a few cases. The intensity of the TUNEL staining was similar or even lower than that observed in the SN.

Apoptosis Inducing Factor
Substantia Nigra

Cytoplasmic localization. In the SN of the human neonate, the majority of neurons displayed granular AIF staining in their cytoplasm and processes, a staining pattern resembling the distribution of mitochondria (Fig. 3A). The cytoplasmic intensity of AIF staining showed particular variability among the neonates of our sample. In the "control" neonate GBB 170/16 (group 0) and some cases of PHI group 1, moderate to intense granular AIF immunoreactivity was observed in the cytoplasm of SN neurons (Fig. 3A). In the other "control" neonate GBB 274/17 (group 0) and the remaining cases of group 1, SN neurons exhibited weak cytoplasmic AIF staining (Fig. 3B). In the majority of PHI group 2 and 3 cases (9/13), SN neurons displayed intense levels of cytoplasmic AIF immunoreactivity (Fig. 3C), whereas in a limited number of neurons a light nuclear AIF reaction was evident (Fig. 3C, arrows).

In the 2 adult control cases, SN melanized neurons showed very light cytoplasmic AIF immunoreaction, while in the Parkinsonian patient, SN neurons were AIF-negative (results not shown).
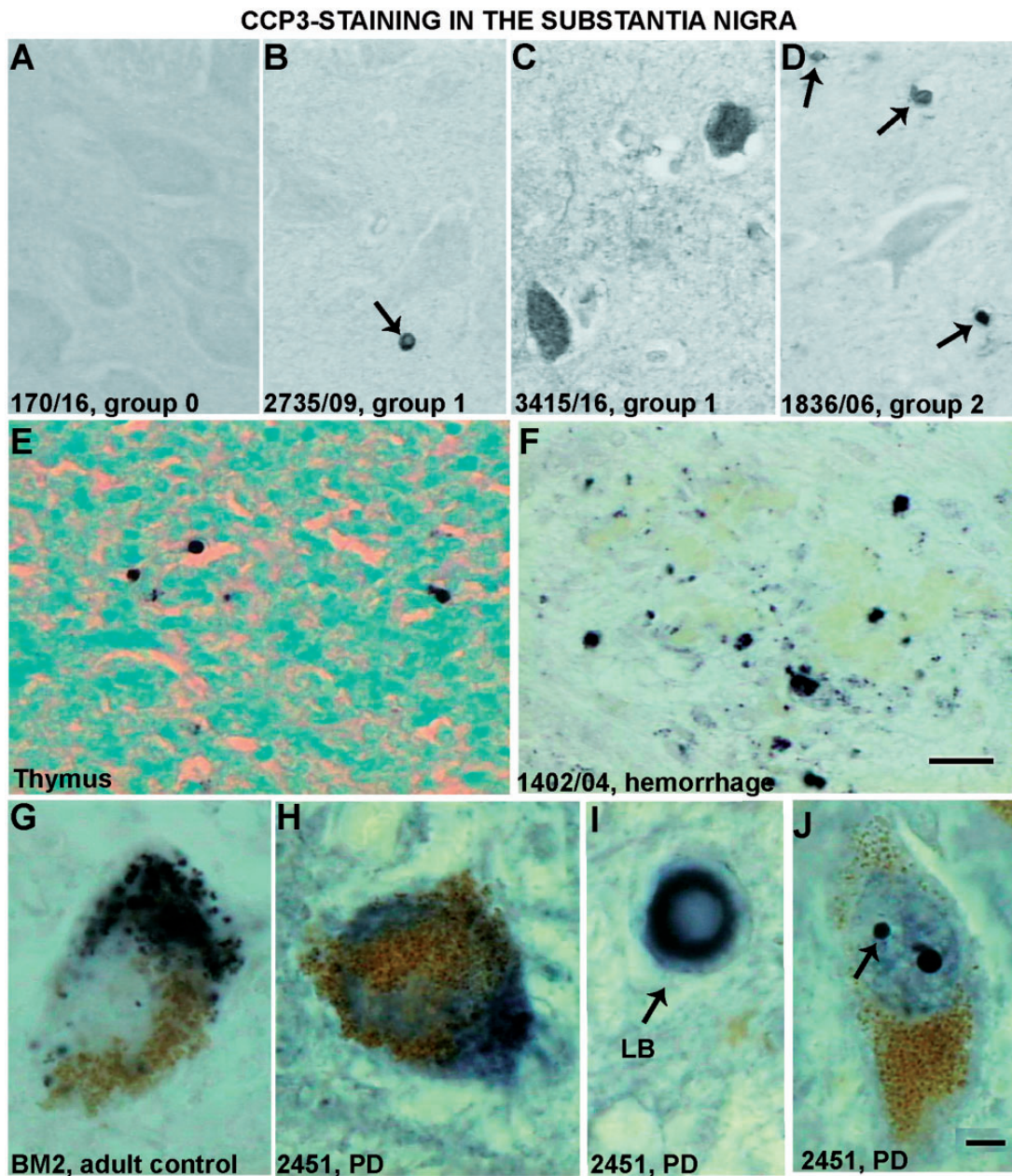
CCP3-STAINING IN THE SUBSTANTIA NIGRA

FIGURE 1. Cleaved caspase-3 (CCP3)-immunohistochemical reaction in the human substantia nigra (SN) and thymus (control tissue for apoptosis). **(A, B)** No CCP3 staining is observed in SN neurons of neonates GBB 170/16 (group 0) and GBB 2735/09 (group 1), respectively. **(B)** Note that only one glial cell is CCP3-positive (arrow) among unstained neurons. **(C)** Exceptionally, few intensely CCP3-stained neurons are revealed in the SN of GBB 3415/16 with genetic skeletal dysplasia (group 1). **(D)** In neonate 1836/06 (Ivemark's syndrome), many glial cells are labeled for CCP3 in SN (arrows). **(E)** Intensely CCP3-stained cells are frequently observed in the human thymus, used as a positive control apoptotic tissue (light green counterstaining). **(F)** In neonate GBB 1402/04, many apoptotic CCP3-positive cells are revealed in a hemorrhagic area in the midbrain (internal positive control of CCP3 staining). **(G)** In a control adult case, SN neurons with neuromelanin (natural color brown) exhibit an intense granular CCP3 staining (black). **(H)** In adult case 2451 with Parkinson disease (PD) and dementia, black CCP3 staining is occasionally found in neurons with neuromelanin (brown). Note the CCP3-positive staining in Lewy bodies (LB) **(I)** and in spherical nuclear inclusions in some apparently healthy melanized SN neurons **(J, arrows),** possibly corresponding to Marinesco bodies. Scale bars: **(A–F)** = 20 μm and **(G–J)** = 5 μm.

The morphometric analysis of the SN neurons without nuclear AIF staining revealed that neonates with evidence of peripheral and/or brain infection displayed higher values of AIF OD in their cytoplasm ($\rho = 0.477$, p = 0.029; Fig. 3M). Statistically significant correlation was also found between the neuronal and nuclear size with the gestational age ($\rho = 0.768$,
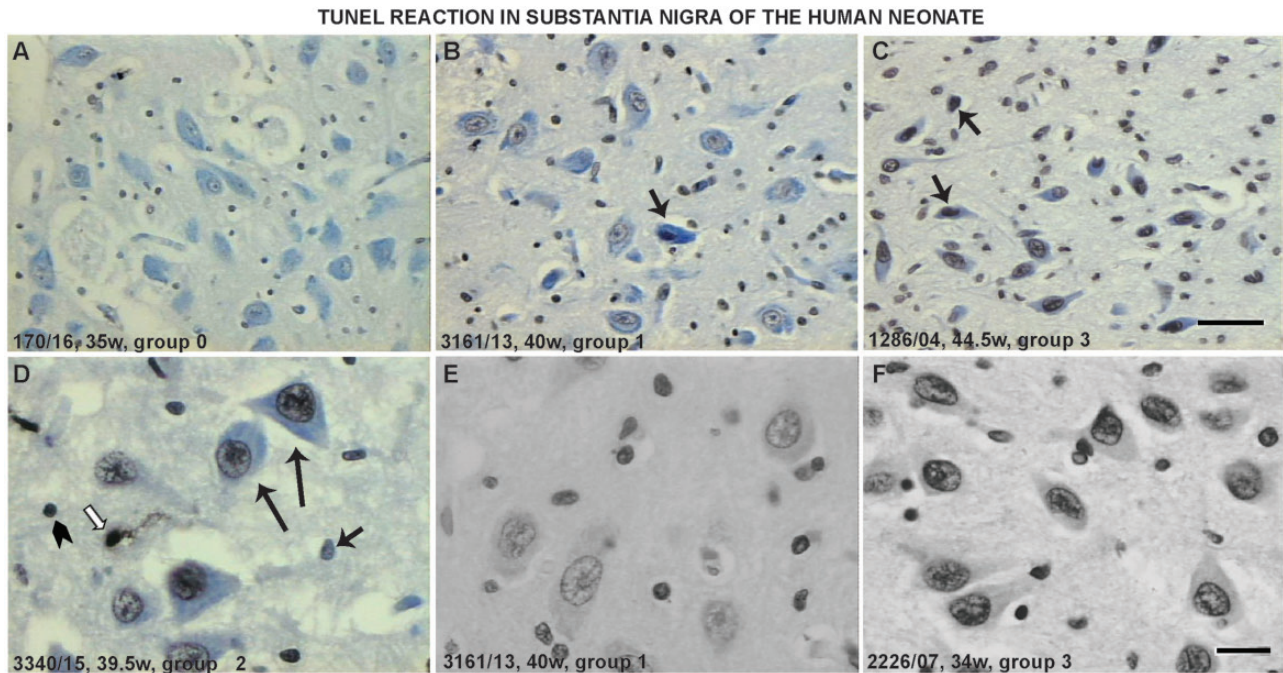
TUNEL REACTION IN SUBSTANTIA NIGRA OF THE HUMAN NEONATE

FIGURE 2. TUNEL staining (methylene blue counterstaining) in the substantia nigra (SN) of the human neonate. **(A)** In the "control" GBB 170/16, no TUNEL-positive nuclei are observed, whereas many glial cells show black TUNEL staining. **(B)** In GBB 3161/13 (group 1), many neurons have a light, diffuse TUNEL staining that outlines their nuclei. One pyknotic neuron (arrow) exhibits intense and condensed labeling, indicative of the apoptotic morphology. **(C)** In GBB 1286/04 (group 3), note the substantial increase in the intensity of the TUNEL staining. Note neurons with intense, dense TUNEL-labeled apoptotic nuclei (arrows). **(D)** In GBB 3340/15 (group 2), a higher magnification reveals the presence of TUNEL-positive nuclei that show a non-apoptotic morphology (loosely chromatin labeling, see long black arrows). Glial cells also exhibit intense TUNEL labeling with differences in the nuclear staining pattern: some glia cells show intense, dense TUNEL staining, indicative of apoptosis (thick, arrowhead), others show diffuse, loose TUNEL labeling, indicative of a non-apoptotic morphology (short arrow) and few are stained in both their soma and processes, corresponding to necrotic features (white arrow). **(E, F)** Higher magnification of SN neurons in neonates 3161/13 (group 1) and 2226/07 (group 3) confirms that TUNEL staining is more intense in group 3 case, although both neonates have similar postmortem delay (≤1 day) (no counterstaining). Scale bars: **(A–C)** = 50 μm and **(D–F)** = 20 μm.

p < 0.001; ρ = 0.764, p < 0.001), postnatal age (ρ = 0.469, p = −0.027; ρ = 0.482, p = −0.023), and brain weight (ρ = 0.776, p < 0.001; ρ = 0.816, p < 0.001, respectively). No correlation was found between the above parameters with PHI grading, sex, postmortem delay, or fixation time.

Nuclear localization. Neurons with apparent nuclear AIF staining (Fig. 3D, white arrow) usually showed a similar cytoplasmic staining compared to neurons with unstained nucleus (compare neighboring neurons in Fig. 3D, E, white arrows). Neurons with light nuclear AIF staining, however, did not present pyknosis or shrinkage in H&E-stained sections (Fig. 3E, F, respectively). Neurons with dark nuclear AIF staining usually had an intense AIF staining surrounding the perinuclear area (Fig. 3G, H, arrows). Small cells with condensed nuclear AIF staining with advanced cytoplasmic shrinkage were rarely found (Fig. 3I). Pyknotic structures intensely stained with AIF were also found (Fig. 3G and compare Fig. 3K with Fig. 3L, arrows).

Oculomotor Nucleus

Cytoplasmic localization. Cytoplasmic AIF staining was seen in many neurons of the oculomotor nucleus and other midbrain

nuclei, such as ventral tegmental area (including paranigral and parabrachial nucleus), superior colliculi, and raphe. Impressively, motor neurons of the oculomotor nucleus showed very strong cytoplasmic AIF immunoreactivity, much higher than that observed in the SN neurons (Fig. 4, compare Fig. 4A–C with Fig. 3A–C, respectively) or other midbrain areas of the same case.

Nuclear localization. Neurons with nuclear AIF positivity were more frequently and readily recognized in the oculomotor nucleus than in the SN (Fig. 4A–C, arrows), even in the "control" cases with no evidence of neuropathological PHI injury (group 0, Fig. 4A, arrow). In the adjacent TUNEL-stained sections, however, these neurons seemed to have non-apoptotic morphology, presenting a diffuse, loose nuclear TUNEL labeling (Fig. 4, compare Fig. 4D with Fig. 4E, white arrows).

Wilcoxon test verified our above observations between SN and oculomotor neurons. The cytoplasmic AIF OD and the percentage of neurons with nuclear AIF staining were statistically significantly higher in the oculomotor nucleus than in the SN (Z = −3.413, p = 0.001, Fig. 4F and Z = −3.621, p < 0.001, Fig. 4G, respectively).
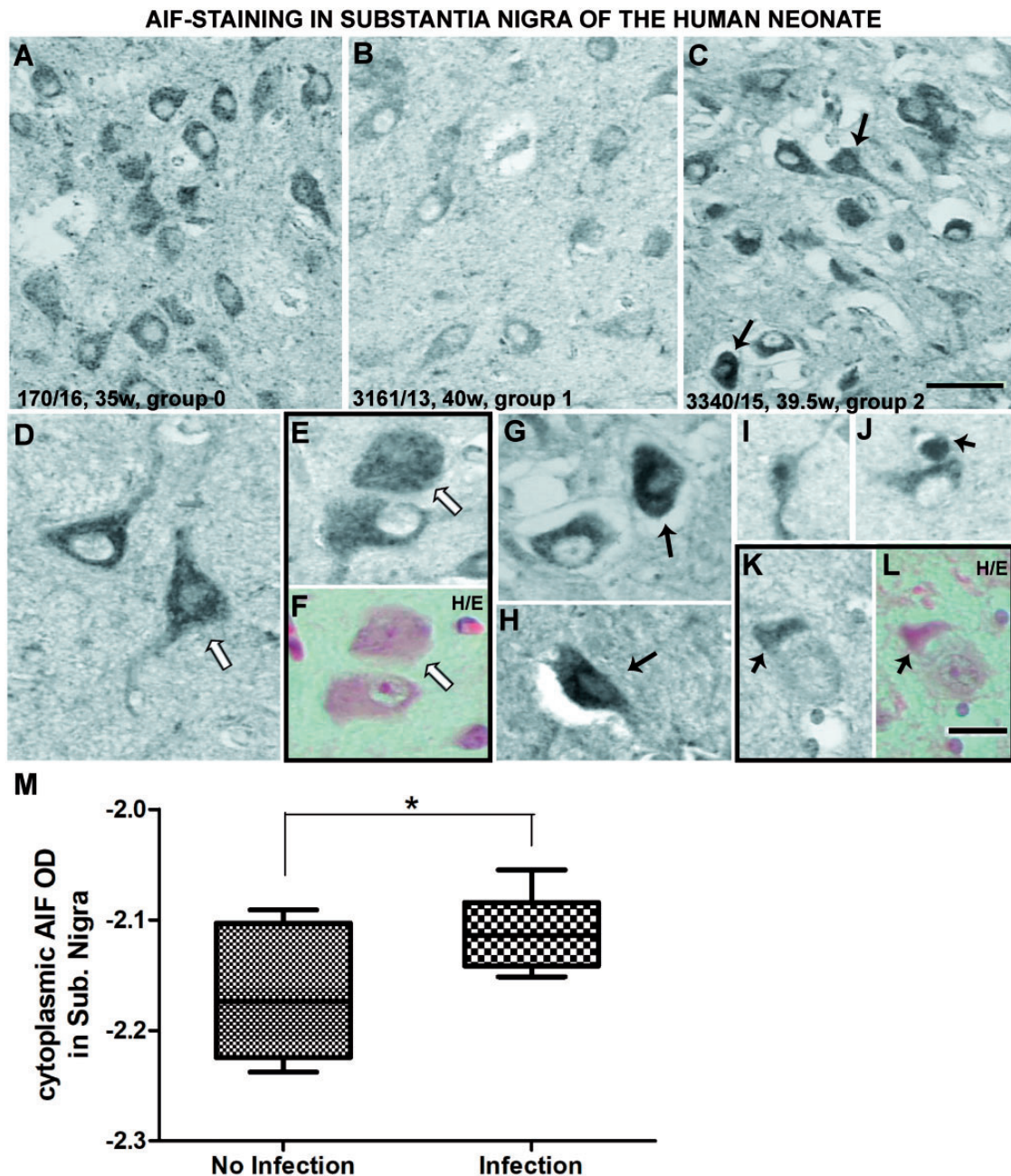
93

FIGURE 3. Apoptosis inducing factor (AIF) staining patterns in the SN neurons of the human neonate. **(A)** In the "control" GBB 170/16 (group 0), SN neurons express high levels of AIF in their cytoplasm. **(B)** In neonate GBB 3161/13 (group 1), the intensity of AIF immunoreactivity is low in the SN neurons. **(C)** In neonate 3340/15 (group 2), SN neurons are more intensely stained for AIF as compared with GBB 3161/13 (group 1). Some neurons show AIF staining in both nucleus and cytoplasm (arrows). **(D)** The neuron marked with the white arrow displays a light AIF immunoreactivity in its nucleus, but the intensity of AIF in its cytoplasm is similar to that observed in the neighboring neuron with unstained nucleus. **(E, F)** Neurons first stained with hematoxylin and eosin (H/E) **(F)**, destained and restained with AIF **(E)**. The neuron with the light nuclear AIF staining **(E, arrow)** did not present pyknosis or shrinkage in H/E staining **(F, arrow)**. **(G, H)** Neurons with dark nuclear AIF staining (arrows) also show intense cytoplasmic staining, especially in the perinuclear area, as compared to a neighboring neuron with unstained nucleus in **(G)**. **(I)** Small cells presenting an intense, condensed nuclear AIF staining with cytoplasmic shrinkage are rarely observed in the SN. Oval **(J)** or irregular AIF-stained structures **(K)** are also observed in the SN of some subjects. These structures appeared to correspond to cells with pyknosis in H/E-stained sections **(L, arrow)**. **(M)** A graph showing that neonates with a peripheral and/or brain infection display more intense AIF immunostaining than neonates without infection ($\rho = 0.477$, $p = 0.029$). The segment inside the rectangle indicates the means (No Infection $= -2.166 \pm 0.016$ and Infection $= -2.111 \pm 0.011$) and "whiskers" above and below the box show the locations of the minimum and maximum. Scale bars: **(A–C)** $= 50\,\mu m$ and **(D–L)** $= 20\,\mu m$.
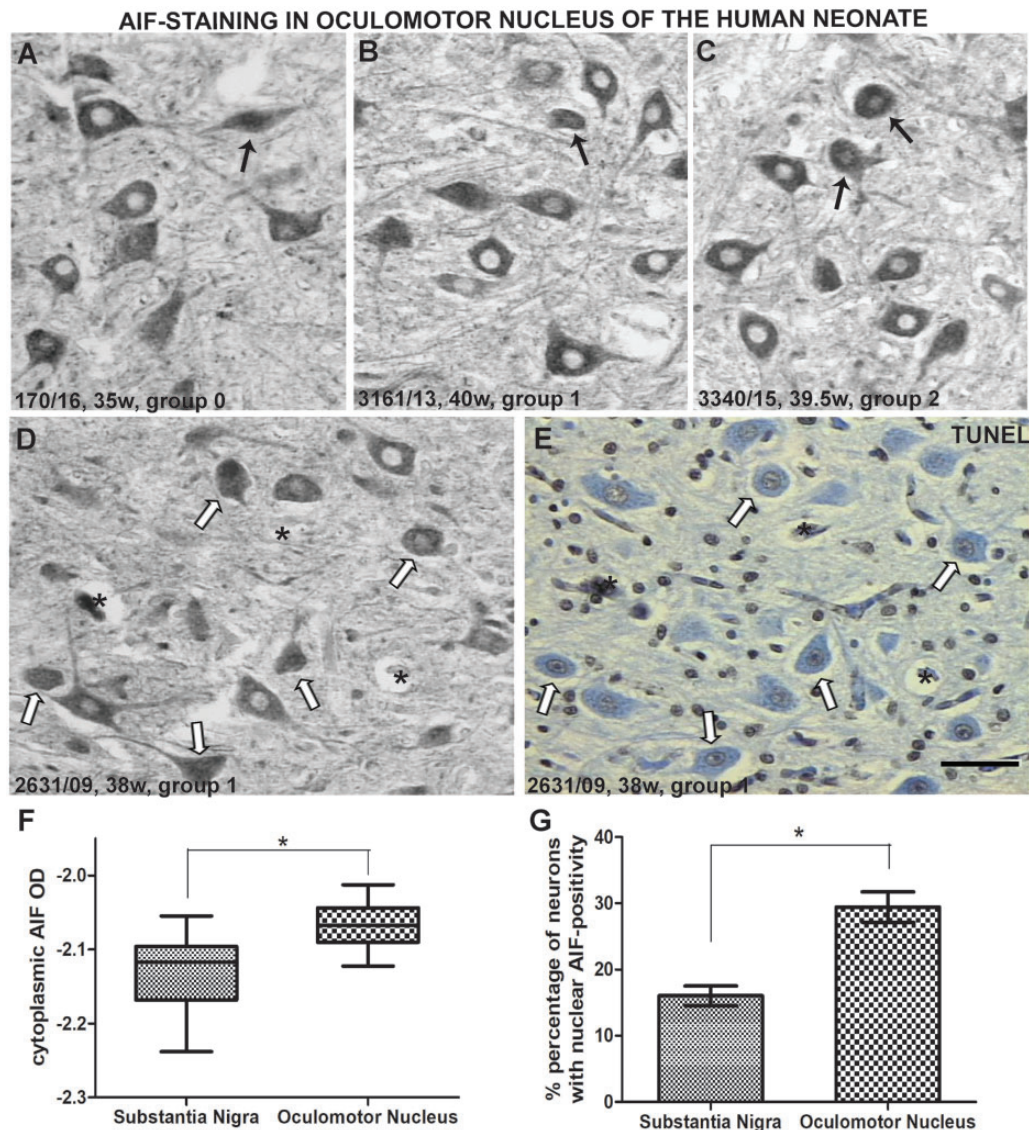
FIGURE 4. AIF immunostaining in the oculomotor nucleus of the human neonate. **(A–C)** The oculomotor nucleus of the same subjects presented in Figure 3A–C. Motor neurons are always more intensely AIF-stained as compared with SN neurons. This did not depend on perinatal hypoxic/ischemic (PHI) grading. Note that neurons displaying nuclear AIF immunoreactivity are more frequently observed in the oculomotor nucleus of all cases studied (arrows). **(D, E)** Parallel sections from the neonate GBB 2631/09 (group 1) stained for AIF and TUNEL, respectively. Neurons showing moderate levels of AIF staining in their nuclei (**D**, white arrows) present a diffuse, loose TUNEL-positive staining (non-apoptotic nuclear morphology, **E**, white arrows). Asterisks show the location of the same blood vessel in the 2 adjacent sections. Bar = 50 μm. **(F)** A graph comparing the cytoplasmic AIF optical density (OD) values measured in SN (means ± SEM = −2.132 ± 0.010) with those in the oculomotor neurons (−2.067 ± 0.008). Statistically significant higher AIF OD was found in oculomotor neurons (Z = −3.413; p = 0.001). **(G)** The means values with SEM of the percentages of neurons with nuclear AIF positivity in the SN (16.04 ± 1.5%) and oculomotor nucleus (29.43 ± 2.3%). Higher numbers of neurons with nuclear AIF staining are measured in the oculomotor nucleus (Z = −3.621, p < 0.001).

The morphometric analysis of our results in the oculomotor nucleus revealed a positive correlation between cytoplasmic or nuclear AIF OD and postmortem delay ($\rho = 0.578$, p = 0.019). In neurons without nuclear AIF staining, the cellular and nuclear size were found to correlate with the gestational age ($\rho = 0.558$, p = 0.020; $\rho = 0.521$, p = 0.032) and brain weight ($\rho = 0.769$, p < 0.001; $\rho = 0.665$, p = 0.004,

respectively). Notably, neurons with nuclear AIF staining showed increased cytoplasmic AIF OD (Z = −2.637, p = 0.008; Fig. 5A) and smaller cellular (Z = −2.533, p = 0.011; Fig. 5B) and nuclear size (Z = −3.574, p < 0.001; Fig. 5C) than the neurons without AIF nuclear staining. No sex differences were observed between the studied apoptotic markers in both SN and oculomotor nucleus, in contrast to

95

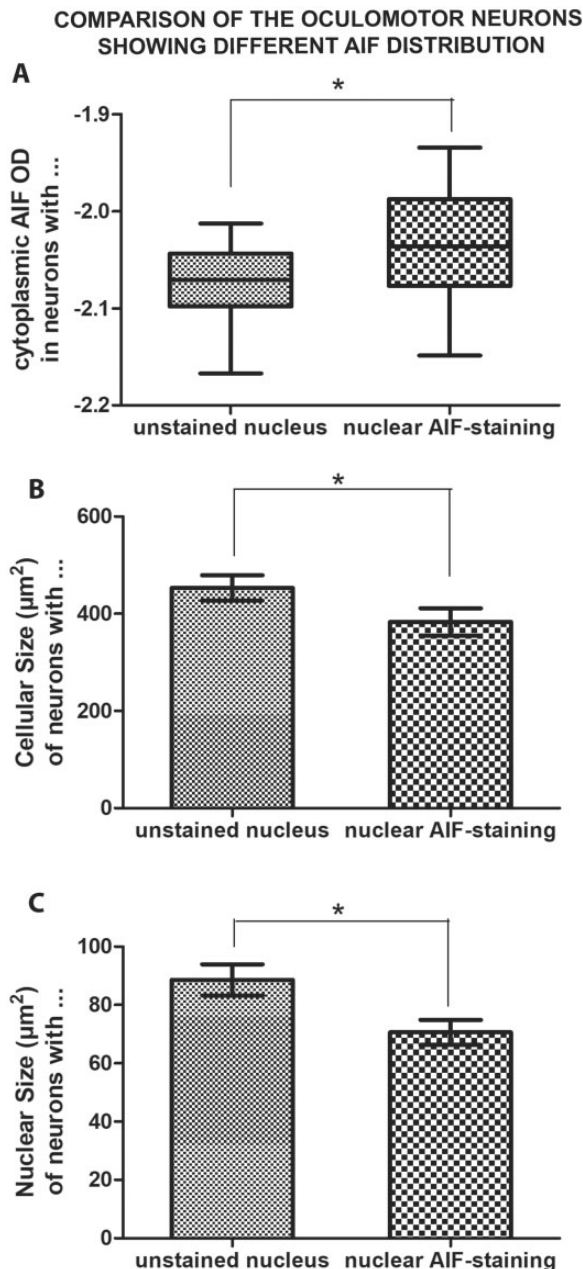## COMPARISON OF THE OCULOMOTOR NEURONS SHOWING DIFFERENT AIF DISTRIBUTION

FIGURE 5. Comparison of oculomotor neurons with different AIF distribution. **(A)** A graph showing the distribution of cytoplasmic AIF optical density (OD) values as measured in neurons with unstained (means $\pm$ SEM = -2.074 ± 0.010) and AIF-stained nucleus (-2.034 ± 0.014). Higher AIF OD values are observed in neurons with AIF-stained nucleus ($Z = -2.637$, $p = 0.008$). **(B, C)** Plots presenting the mean cellular and nuclear sizes with SEM, respectively, of neurons with unstained (453 ± 26 and 89 ± 5) and AIF-stained nucleus (383 ± 28 and 71 ± 4). Note that neurons with AIF staining in the nucleus have significantly smaller cellular and nuclear sizes than those with unstained nucleus ($Z = -2.533$, $p = 0.011$; $Z = -3.574$, $p < 0.001$).

data reported for other brain areas in experimental PHI studies (33, 34). Our immunohistochemical results are summarized in Table 3.

DISCUSSION

To our knowledge, this is the first time that the apoptotic markers CCP3 and AIF, as well as DNA fragmentation (by using TUNEL method), were studied in the midbrain of the human neonate, providing new insights on the brain apoptotic mechanisms following PHI neuropathological injury. Our main results showed limited neuronal degeneration in the SN, mainly mediated by the effector molecule AIF and not by CCP3. By contrast, early signs of degeneration were extensively observed in the oculomotor nucleus indicated by increased cytoplasmic and nuclear translocation of AIF.

CCP3 Expression in the SN

Caspase-dependent apoptosis is a prominent death mechanism occurring during normal brain development, being involved in the discrete elimination of a large number of cells aiming to brain tissue ramification (35). Caspase-dependent apoptotic mechanisms are also important in the evolution of hypoxic/ischemic (HI) injury in the immature brain. Caspase-3, the most abundant apoptotic effector caspase in the brain (35), is massively activated in many rat brain areas (e.g. cerebral cortex, hippocampus, thalamus, and striatum) immediately after experimentally induced hypoxia/ischemia at postnatal day 7, the age that is considered comparable to late preterm/term human neonate (36–40). Generally, in these injured areas, CCP3 is detectable early after the HI insult and its levels peak at 24 hours, then decrease but remain detectable even after 6 days post-HI (36, 38–40).

In SN, increased number of CCP3-IR neurons has been reported in preterm lambs after umbilical cord occlusion causing severe fetal asphyxia during late-gestation (18). Cell death with apoptotic features, as indicated by silver staining and in situ 3′-end-labeling of DNA, has been described in the rat SN after PHI injury (17). In our study, however, CPP3 immunoreactivity was only observed in few glial cells, while neurons in SN, as well as other mesencephalic neuronal groups of human neonates, were generally negative, a result confirmed by 2 different commercially provided antibodies. This unexpected observation cannot be attributed to the effect of postmortem delay or fixation time, since CCP3 staining was observed in a limited number of glial cells being more abundant in the neonatal brain in areas with hemorrhages, as described in the adult brain after hemorrhagic stroke (41). In addition, some CCP3-IR neurons or glia were respectively observed in 2 neonates of our sample, that is, GBB 3415/16 with a genetic inherited skeletal ciliopathy (Ellis van Creveld [EvC] syndrome/chondroectodermal dysplasia/OMIM #225500) and GBB 1836/06 with Ivemark syndrome (heterotaxy syndrome/asplenia with cardiovascular anomalies), a syndrome of obscure and heterogeneous etiology, mostly sporadic and only occasionally inherited (NORD-Rare Disease Database; OMIM #208530). Concerning EvC syndrome, although certain skeletal ciliopathies may feature brain defects, particularly of the posterior fossa, the brain in fetuses with EvC syndrome is normal, while motor development and intelligence are normal in survivors (OMIM #225500; NORD-Rare Disease Database). Similarly, brain disorders are not typical for Ivemark syndrome, although agenesis of the corpus callosum with pachygyria and hydro-

TABLE 3. Summary of the Immunohistochemical Results Observed by CCP3, TUNEL, and AIF Staining in Neurons of Substantia Nigra and Oculomotor Nucleus of Human Neonates With Different PHI Grading

Region	PHI Grading	CCP3	TUNEL		AIF	
			Intensity	Nuclear Morphology	Cytoplasmic Intensity	Nuclear Translocation
Substantia nigra	Control	–	–	–	Variable	Very few
	Group 1	–	Light	Outlying nucleus and nucleolus	Variable	Very few
	Groups 2–3	–	Intense	Diffuse, loose chromatin	Intense	Few
Oculomotor nucleus	Control	–	–	–	Intense	Many
	Group 1	–	Light	Outlying nucleus and nucleolus	Intense	Many
	Groups 2–3	–	Intense	Diffuse, loose chromatin/few with dense chromatin	Intense	Many

–, no staining; AIF, apoptosis inducing factor; CCP3, cleaved caspase-3; PHI, perinatal hypoxia/ischemia.

cephalus have been rarely reported (42); these defects were not found in our case. Given the rarity and diversity of these diseases, detailed information on brain pathology and neurophysiology is too limited to draw any conclusions.

CCP3 immunostaining was revealed in the adult control and degenerating SN. In control cases, SN neurons exhibited a cytoplasmic granular CCP3 staining intermingled with melanin granules, as previously described, probably reflecting a perimortem phenomenon related to hypoxia secondary to the patients' agonal state (32). In addition, CCP3-IR neurons and glial cells have been reported in the SN of patients with Parkinson disease (32, 43, 44), supporting caspase's-3 role in apoptosis of degenerating SN neurons. In our study, we detected intense CCP3 staining in few melanized neurons of Parkinsonian SN, as well as within Lewy bodies, confirming the observation of Hartmann et al (32). Interestingly, in this Parkinsonian case, CCP3 positivity was also revealed in round intranuclear inclusions, probably corresponding to Marinesco bodies. Marinesco bodies have been reported to contain various proteins, such as ubiquitin and GAPDH (43, 45), but not CCP3.

Caspase-3 appears to be strongly regulated by age (36, 40, 46–48). In rats, caspase-3 is normally highly expressed in the developing brain (40) but significantly decreased after postnatal days 10–13 (corresponding to neonatal human brain), when neurogenesis and synaptogenesis are completed (36, 46). Thus, developing neurons appear to be more prone to caspase-dependent apoptotic death than mature ones (36, 37, 39, 40). In rat SN, naturally occurring neuronal apoptosis takes place in a biphasic way. It presents 2 peaks, one at postnatal day 2 and another at postnatal day 14—corresponding to premature and neonatal human brains, respectively (49, 50). Since the rat SN reaches the adult distribution of TH-IR neurons by postnatal day 14 (50, 51), the first 2 weeks of rat life are crucial for the establishment of the final number of neuron and glia cells that form and control the dopaminergic circuitry in the rat brain (52, 53). In humans, however, dopaminergic neurons of SN reach the overall adult distribution pattern, as assessed by TH expression, prenatally at the fourth month of gestation (54). In 20- to 24-week-old human fetuses, widespread TH-positive innervation of the frontal cortex is observed comparable to that of the adult (54). Given that the

corrected (prenatal and postnatal) age of our subjects ranged from 25.5 to 46.5 weeks, a "mature" dopaminergic system was expected in the neonates of our sample, as also mentioned in our previous study with TH-immunohistochemistry (19). Therefore, the absence of immunohistochemically detectable CCP3 could simply indicate that CCP3 may no longer be needed in SN neurons of the human neonate, possibly due to downregulation of the apoptotic machinery at this developmental stage.

TUNEL Labeling in the SN

Our findings on CCP3 were consistent with the results obtained by TUNEL staining, which is extensively used in PHI models for the detection of DNA fragmentation occurring at a later stage in the apoptotic process (22, 23, 55–59). In our study, very few SN neurons were observed with nuclear TUNEL labeling with apoptotic morphology, that is, nuclear condensation, margination and clumping of chromatin, along with pyknotic cytoplasm. Most neurons displayed a diffuse, loose nuclear TUNEL labeling considered to be unrelated to apoptosis, the intensity of which appeared to be dependent on PHI grading. In contrast, a variety of TUNEL-positive nuclear morphologies (i.e. apoptotic, non-apoptotic, and necrotic) were observed in glial cells of our sample, indicative of inflammatory glial responses after PHI (60, 61). Non-apoptotic TUNEL-labeled figures have been extensively described in human control and degenerative brain tissues (62–66), considered to reflect the combined action of accelerated DNA damage and/or defective DNA repair, with activation or arrest of aspects of the apoptotic program (62, 64). Indeed, it is now widely accepted that TUNEL technique is not entirely specific for apoptosis and must be combined with the investigation of other apoptosis-related markers in order to accurately define whether apoptotic mechanisms are activated or not. Therefore, TUNEL method could also label cells in which DNA fragmentation has occurred by other mechanisms including necrosis, autolysis, and possibly other metabolic cellular insults or processes involving unwinding of DNA strands, such as cytotoxic agents, growth factor deprivation, and free radicals (62, 64, 65, 67–69). In addition, TUNEL staining seems to be greatly affected by methods and conditions of tissue processing and

97

storage, such as postmortem intervals >72 hours and tissue fixation in 10% formalin for >2 years (23, 62, 63, 65, 68, 70). Since almost all brain tissues of our sample were obtained within the above intervals, we assumed that these 2 factors may have had only little effect on our TUNEL staining. We speculate that the observed non-apoptotic figures might mainly reflect the result of antemortem hypoxia, as was similarly supported by Kingsbury et al (71). Interestingly, the integrity of DNA could recover post-hypoxia, as observed in various brain areas of newborn hypoxic piglets (56), implying that DNA fragmentation could be repaired by the endogenous DNA repairing mechanisms and, therefore, be a reversible phenomenon (72). However, extensive DNA damage could cause the activation of a unique poly(ADP-ribose) polymerase (PARP-1)-dependent cell death program, which is independent of caspases but dependent on AIF (73, 74).

AIF Expression in the SN: Cytoplasmic Versus Nuclear Localization

AIF plays a dual life/death role. It is normally confined to the mitochondrial intermembrane space where it promotes cell survival, whereas it initiates its cell death program after its translocation to the nucleus (for review, [24]). These opposing roles could be immunohistochemically studied by focusing on the different expression patterns of AIF within a cell, that is, the cytoplasmic localization of AIF is mainly related with its mitochondrial life-promoting function, whereas AIF staining in the nucleus is associated with its death function. Since both expression patterns were observed in our study, we separately investigated these 2 "different" neuronal populations by measuring and comparing their morphological and staining characteristics.

In the SN, the majority of neurons displayed cytoplasmic AIF immunoreactivity, the intensity of which displayed particular variability among the subjects of our sample, even between the 2 "control" neonates. Since AIF is normally involved in the maintenance and/or organization of the mitochondrial respiratory complex I (for review, [24]), the observed variability could simply reflect interindividual differences in SN metabolic/energy state under a mixed genetic background (75). However, AIF immunoreactivity tended to be higher in neonates with group 2 or 3 PHI grading, the majority of which also showed evidence of peripheral or brain infection. Recent studies suggested that both infection and PHI could lead to brain damage via common cellular and molecular pathways, involving the generation of reactive oxygen species and thus, lower the threshold at which PHI alone triggers brain injury (76–79). Since AIF could also act as a free radical scavenger, by displaying NADH oxidoreductase and peroxide scavenging activities (80, 81), this increased AIF expression in SN neurons of certain cases could be a compensatory mechanism against the increased oxidative stress and free radical production caused by inflammation and/or PHI. High AIF levels could, however, render neurons more vulnerable to death, given that downregulation of AIF significantly reduces brain damage (82–84). Interestingly, in the adult rat, SN neurons have been reported to undergo death through AIF after inflammation caused by either intranigral or systemic lipopolysaccharide administration (85, 86). In humans, dopaminergic neurons appeared to contain more AIF than mice and monkeys, thus SN neurons are expected to be more sensitive to AIF-mediated death (87).

Experimental studies report extensive translocation of AIF after PHI, mainly in the cerebral cortex and hippocampus (33, 34, 88–90). Neurons entering an AIF-dependent death program first show a marked increase of AIF in their neuronal cytoplasm, close to the nuclear envelope, before AIF enters the nucleus. Nuclear staining is then gradually increasing with time, becomes more condensed, and eventually outlines pyknotic nuclei (90–92). In our study, neurons with nuclear AIF staining were occasionally found in SN. These neurons displayed a dark nuclear AIF staining with intense perinuclear AIF expression and had significantly smaller sizes. Many neurons having a light nuclear AIF staining did not present any changes in their morphology and cytoplasmic AIF content, raising the question whether this light nuclear AIF staining represents a real early phase of nuclear translocation. Plesnila et al (91) mention that after focal cerebral ischemia, cortical neurons maintain their normal nuclear morphology and size for hours before becoming shrunken, although AIF has been already translocated in their nucleus.

Translocation of AIF in the nucleus frequently causes a large-scale DNA degradation and consequently induces chromatin condensation (90, 92, 93). Paradoxically, in our study, the majority of neurons with light or dark nuclear AIF staining showed a non-apoptotic nuclear morphology in TUNEL-stained sections. AIF translocation to the nucleus could occur independently of the intracellular ATP levels (94) and may be facilitated by the increased permeability of the nuclear pore complex during cell death (95). ATP concentration, however, could determine whether cells will execute the final phase of apoptosis that involves nuclear condensation and DNA fragmentation (94, 96). Thus, cells under ATP depletion fail to manifest any signs of chromatin condensation and advanced DNA fragmentation, although they present AIF nuclear staining and reduction of nuclear size (94, 96), as also observed in our sample.

In the absence of caspase-3 activation, release and nuclear translocation of AIF have been observed in the dopaminergic neurons of rodent SN after injury induced by rotenone (97), 6-hydroxydopamine (98), or MPTP injection (99), used as experimental models of Parkinson disease. Interestingly, in the 6-hydroxydopamine experimental model, SN dopaminergic neurons with nuclear AIF translocation usually exhibited reduced levels of TH expression (98), that could only partially explain our previously observed massive downregulation of TH expression in SN neurons of the human neonate under PHI (19). Nuclear translocation of AIF has also been described in the degenerating SN neurons from subjects with Parkinson disease (85).

AIF Expression in the Oculomotor Nucleus: Cytoplasmic Versus Nuclear Localization

Our results showed that AIF expression is not exclusive for the dopaminergic neurons, since other mesencephalic neuronal groups also displayed AIF staining, such as oculomotor

nucleus and superior colliculi, 2 subcortical structures involved in the eye orientation network (100). Oculomotor neurons displayed significantly higher cytoplasmic AIF immunoreactivity and AIF nuclear translocation than the SN or the reported hypoxia-sensitive superior colliculi (101). This could be related either to the high energy needs of oculomotor neurons—indicated by their high expression of cytochrome oxidase (102)—or to their increased sensitivity to oxidative damage—depicted by their high content in the antioxidant copper/zinc superoxide dismutase (SOD-1) (103). In addition, our results indicated that AIF immunoreactivity in oculomotor nucleus increased after prolonged postmortem delay, an observation not revealed in SN neurons. Postmortem events, including increased mitochondrial swelling, reactive oxygen species production, and release of lysosomal enzymes, have been reported to cause AIF nuclear translocation in the bovine muscle, a tissue with also high energy demands (104).

In the oculomotor nucleus of the human neonate, extremely high percentages (>25%) of neurons showed nuclear AIF translocation combined with smaller cellular and nuclear sizes. These probable early signs of degeneration could be part of the normal developmental apoptotic processes, as described in humans (105, 106).

The oculomotor nucleus innervates 4 extraocular muscles and thus is involved in the control of eye movements, such as saccades, vestibular ocular reflexes, and optokinetic responses (100). Interestingly, oculomotor disturbances, including defective coordination of saccades, are frequently observed in newborns and children following perinatal hypoxia (107–109), as well as in patients with schizophrenia, ADHD, and Parkinson disease (110, 111), disorders in which PHI is considered as an important risk factor.

Conclusions

Our results mainly indicate the activation of AIF but not CCP3 in the SN and the oculomotor nucleus of human neonates with neuropathological signs of PHI lesions, despite the heterogeneity of the available human postmortem material regarding autolysis and fixation time.

In the SN, inflammation through its synergistic effect with PHI appeared to be related to AIF activation. However, a limited number of SN neurons presented AIF nuclear translocation, indicating that only few SN neurons show early signs of AIF-mediated degeneration. The oculomotor neurons appeared to be more prone to AIF-mediated cell degeneration than those of the SN in the human neonate. Higher cytoplasmic AIF expression and nuclear translocation were observed in the oculomotor nucleus, which could be the result of the combined effect of developmental processes in association with the increased oxidative stress induced by antemortem and postmortem factors. Further investigation is needed to clarify this preferential activation of AIF, but not caspase-3, in these midbrain nuclei during the developmentally critical neonatal period.

REFERENCES

1. Millar LJ, Shi L, Hoerder-Suabedissen A, et al. Neonatal hypoxia ischaemia: Mechanisms, models, and therapeutic challenges. Front Cell Neurosci 2017;11:78
2. Faa G, Manchia M, Pintus R, et al. Fetal programming of neuropsychiatric disorders. Birth Defect Res C 2016;108:207–23
3. Giannopoulou I, Pagida MA, Briana DD, et al. Perinatal hypoxia as a risk factor for psychopathology later in life: The role of dopamine and neurotrophins. Hormones (Athens) 2018;17:25–32
4. Mittal VA, Ellman LM, Cannon TD. Gene-environment interaction and covariation in schizophrenia: The role of obstetric complications. Schizophr Bull 2008;34:1083–94
5. Rennie JM, Hagmann CF, Robertson NJ. Outcome after intrapartum hypoxic ischaemia at term. Semin Fetal Neonatal Med 2007;12:398–407
6. Smith TF, Schmidt-Kastner R, McGeary JE, et al. Pre- and perinatal ischemia-hypoxia, the ischemia-hypoxia response pathway, and ADHD risk. Behav Genet 2016;46:467–77
7. Halliday GM, Reyes S, Double K. Substantia nigra ventral tegmental area and retrorubral fields. In: Mai J, Paxinos G, eds. The Human Nervous System. 3rd ed. Waltham, MA: Academic Press 2012: 441–57
8. Luo SX, Huang EJ. Dopaminergic neurons and brain reward pathways: From neurogenesis to circuit assembly. Am J Pathol 2016;186:478–88
9. Rizzi G, Tan KR. Dopamine and acetylcholine, a circuit point of view in Parkinson's disease. Front Neural Circuits 2017;11:110
10. Howes O, McCutcheon R, Stone J. Glutamate and dopamine in schizophrenia: An update for the 21st century. J Psychopharmacol 2015;29:97–115
11. Weinstein JJ, Chohan MO, Slifstein M, et al. Pathway-specific dopamine abnormalities in schizophrenia. Biol Psychiatry 2017;81:31–42
12. Gonon F. The dopaminergic hypothesis of attention-deficit/hyperactivity disorder needs re-examining. Trends Neurosci 2009;32:2–8
13. Boksa P, El-Khodor BF. Birth insult interacts with stress at adulthood to alter dopaminergic function in animal models: Possible implications for schizophrenia and other disorders. Neurosci Biobehav Rev 2003;27:91–101
14. Burke RE, Macaya A, DeVivo D, et al. Neonatal hypoxic-ischemic or excitotoxic striatal injury results in a decreased adult number of substantia nigra neurons. Neuroscience 1992;50:559–69
15. Bjelke B, Andersson K, Ogren SO, et al. Asphyctic lesion: Proliferation of tyrosine hydroxylase-immunoreactive nerve cell bodies in the rat substantia nigra and functional changes in dopamine neurotransmission. Brain Res 1991;543:1–9
16. Chen Y, Herrera-Marschitz M, Bjelke B, et al. Perinatal asphyxia-induced changes in rat brain tyrosine hydroxylase-immunoreactive cell body number: Effects of nicotine treatment. Neurosci Lett 1997;221:77–80
17. Oo TF, Henchcliffe C, Burke RE. Apoptosis in substantia nigra following developmental hypoxic-ischemic injury. Neuroscience 1995;69:893–901
18. Castillo-Melendez M, Chow JA, Walker DW. Lipid peroxidation, caspase-3 immunoreactivity, and pyknosis in late-gestation fetal sheep brain after umbilical cord occlusion. Pediatr Res 2004;55:864–71
19. Pagida MA, Konstantinidou AE, Tsekoura E, et al. Vulnerability of the mesencephalic dopaminergic neurons of the human neonate to prolonged perinatal hypoxia: An immunohistochemical study of tyrosine hydroxylase expression in autopsy material. J Neuropathol Exp Neurol 2013;72:337–50
20. Thornberry NA. Caspases: A decade of death research. Cell Death Differ 1999;6:1023–7
21. Gavrieli Y, Sherman Y, Ben-Sasson SA. Identification of programmed cell death in situ via specific labeling of nuclear DNA fragmentation. J Cell Biol 1992;119:493–501
22. Stadelmann C, Lassmann H. Detection of apoptosis in tissue sections. Cell Tissue Res 2000;301:19–31
23. Hara A, Niwa M, Iwai T, et al. Neuronal apoptosis studied by a sequential TUNEL technique: A method for tract-tracing. Brain Res Brain Res Protoc 1999;4:140–6

24. Bano D, Prehn J. Apoptosis-inducing factor (AIF) in physiology and disease: The tale of a repented natural born killer. EBioMedicine 2018; 30:29–37
25. Pagida MA, Konstantinidou AE, Tsekoura E, et al. Immunohistochemical demonstration of urocortin 1 in Edinger-Westphal nucleus of the human neonate: Colocalization with tyrosine hydroxylase under acute perinatal hypoxia. Neurosci Lett 2013;554:47–52
26. Fallet-Bianco C. Diagnosis and dating of hypoxic-ischemic encephalopathy. Paper from the 20th European Congress of Pathology held in Paris France, September 3–8, 2005.127–32
27. Rorke-Adams L, Larroche J, de Vries L. Fetal and neonatal brain damage. In: Gilbert-Barness E, ed. Potter's Pathology of the Fetus, Infant and Child. Vol. 2. 2nd ed. Philadelphia, PA: Mosby-Elsevier 2007: 2027–53
28. Squier W. Gray matter lesions. In: Golden J, Harding B, eds. Pathology and Genetics, Developmental Neuropathology. Basel, Switzerland: ISN Neuropathology Press 2004:171–5
29. Pagida MA, Konstantinidou AE, Korelidou A, et al. The effect of perinatal hypoxic/ischemic injury on tyrosine hydroxylase expression in the locus coeruleus of the human neonate. Dev Neurosci 2016;38:41–53
30. Paxinos G, Huang XF. Atlas of the Human Brainstem. San Diego: Academic Press 1995
31. Kuida K, Zheng TS, Na S, et al. Decreased apoptosis in the brain and premature lethality in CPP32-deficient mice. Nature 1996;384:368–72
32. Hartmann A, Hunot S, Michel PP, et al. Caspase-3: A vulnerability factor and final effector in apoptotic death of dopaminergic neurons in Parkinson's disease. Proc Natl Acad Sci U S A 2000;97:2875–80
33. Askalan R, Gabarin N, Armstrong EA, et al. Mechanisms of neurodegeneration after severe hypoxic-ischemic injury in the neonatal rat brain. Brain Res 2015;1629:94–103
34. Zhu C, Xu F, Wang X, et al. Different apoptotic mechanisms are activated in male and female brains after neonatal hypoxia-ischaemia. J Neurochem 2006;96:1016–27
35. Blomgren K, Leist M, Groc L. Pathological apoptosis in the developing brain. Apoptosis 2007;12:993–1010
36. Wang X, Karlsson JO, Zhu C, et al. Caspase-3 activation after neonatal rat cerebral hypoxia-ischemia. Biol Neonate 2001;79:172–9
37. Liu CL, Siesjo BK, Hu BR. Pathogenesis of hippocampal neuronal death after hypoxia-ischemia changes during brain development. Neuroscience 2004;127:113–23
38. Carloni S, Carnevali A, Cimino M, et al. Extended role of necrotic cell death after hypoxia-ischemia-induced neurodegeneration in the neonatal rat. Neurobiol Dis 2007;27:354–61
39. Nakajima W, Ishida A, Lange MS, et al. Apoptosis has a prolonged role in the neurodegeneration after hypoxic ischemia in the newborn rat. J Neurosci 2000;20:7994–8004
40. Zhu C, Wang X, Hagberg H, et al. Correlation between caspase-3 activation and three different markers of DNA damage in neonatal cerebral hypoxia-ischemia. J Neurochem 2002;75:819–29
41. Pirici D, Pirici I, Mogoanta L, et al. Matrix metalloproteinase-9 expression in the nuclear compartment of neurons and glial cells in aging and stroke. Neuropathology 2012;32:492–504
42. Noack F, Sayk F, Ressel A, et al. Ivemark syndrome with agenesis of the corpus callosum: A case report with a review of the literature. Prenat Diagn 2002;22:1011–5
43. Tatton NA. Increased caspase 3 and Bax immunoreactivity accompany nuclear GAPDH translocation and neuronal apoptosis in Parkinson's disease. Exp Neurol 2000;166:29–43
44. Burguillos MA, Deierborg T, Kavanagh E, et al. Caspase signalling controls microglia activation and neurotoxicity. Nature 2011;472: 319–24
45. Odagiri S, Tanji K, Mori F, et al. Immunohistochemical analysis of Marinesco bodies, using antibodies against proteins implicated in the ubiquitin-proteasome system, autophagy and aggresome formation. Neuropathology 2012;32:261–6
46. Blomgren K, Zhu C, Wang X, et al. Synergistic activation of caspase-3 by m-calpain after neonatal hypoxia-ischemia: A mechanism of "pathological apoptosis"? J Biol Chem 2001;276:10191–8
47. Hu BR, Liu CL, Ouyang Y, et al. Involvement of caspase-3 in cell death after hypoxia-ischemia declines during brain maturation. J Cereb Blood Flow Metab 2000;20:1294–300
48. Zhu C, Wang X, Xu F, et al. The influence of age on apoptotic and other mechanisms of cell death after cerebral hypoxia-ischemia. Cell Death Differ 2005;12:162–76
49. Janec E, Burke RE. Naturally occurring cell death during postnatal development of the substantia nigra pars compacta of rat. Mol Cell Neurosci 1993;4:30–5
50. Oo TF, Burke RE. The time course of developmental cell death in phenotypically defined dopaminergic neurons of the substantia nigra. Brain Res Dev Brain Res 1997;98:191–6
51. Tepper JM, Damlama M, Trent F. Postnatal changes in the distribution and morphology of rat substantia nigra dopaminergic neurons. Neuroscience 1994;60:469–77
52. Chocyk A, Dudys D, Przyborowska A, et al. Maternal separation affects the number, proliferation and apoptosis of glia cells in the substantia nigra and ventral tegmental area of juvenile rats. Neuroscience 2011;173: 1–18
53. Bandeira F, Lent R, Herculano-Houzel S. Changing numbers of neuronal and non-neuronal cells underlie postnatal brain growth in the rat. Proc Natl Acad Sci U S A 2009;106:14108–13
54. Verney C. Distribution of the catecholaminergic neurons in the central nervous system of human embryos and fetuses. Microsc Res Tech 1999; 46:24–47
55. Dell'Anna E, Chen Y, Engidawork E, et al. Delayed neuronal death following perinatal asphyxia in rat. Exp Brain Res 1997;115:105–15
56. David JC, Grongnet JF. Effect of hypoxia on DNA fragmentation in different brain regions of the newborn piglet. Mol Reprod Dev 2000;57: 153–8
57. Takada SH, dos Santos Haemmerle CA, Motta-Teixeira LC, et al. Neonatal anoxia in rats: Hippocampal cellular and subcellular changes related to cell death and spatial memory. Neuroscience 2015;284:247–59
58. Hernandez-Jimenez M, Sacristan S, Morales C, et al. Apoptosis-related proteins are potential markers of neonatal hypoxic-ischemic encephalopathy (HIE) injury. Neurosci Lett 2014;558:143–8
59. Scott RJ, Hegyi L. Cell death in perinatal hypoxic-ischaemic brain injury. Neuropathol Appl Neurobiol 1997;23:307–14
60. Benjelloun N, Renolleau S, Represa A, et al. Inflammatory responses in the cerebral cortex after ischemia in the P7 neonatal Rat. Stroke 1999; 30:1916–23;discussion 23-4
61. Ezquer ME, Valdez SR, Seltzer AM. Inflammatory responses of the substantia nigra after acute hypoxia in neonatal rats. Exp Neurol 2006; 197:391–8
62. Anderson AJ, Stoltzner S, Lai F, et al. Morphological and biochemical assessment of DNA damage and apoptosis in Down syndrome and Alzheimer disease, and effect of postmortem tissue archival on TUNEL. Neurobiol Aging 2000;21:511–24
63. Anderson AJ, Su JH, Cotman CW. DNA damage and apoptosis in Alzheimer's disease: Colocalization with c-Jun immunoreactivity, relationship to brain area, and effect of postmortem delay. J Neurosci 1996;16: 1710–9
64. Gleckman AM, Jiang Z, Liu Y, et al. Neuronal and glial DNA fragmentation in Pick's disease. Acta Neuropathol 1999;98:55–61
65. Lucassen PJ, Chung WC, Vermeulen JP, et al. Microwave-enhanced in situ end-labeling of fragmented DNA: Parametric studies in relation to postmortem delay and fixation of rat and human brain. J Histochem Cytochem 1995;43:1163–71
66. Vis JC, Schipper E, de Boer-van Huizen RT, et al. Expression pattern of apoptosis-related markers in Huntington's disease. Acta Neuropathol 2005;109:321–8
67. Grasl-Kraupp B, Ruttkay-Nedecky B, Koudelka H, et al. In situ detection of fragmented DNA (TUNEL assay) fails to discriminate among apoptosis, necrosis, and autolytic cell death: A cautionary note. Hepatology 1995;21:1465–8
68. Labat-Moleur F, Guillermet C, Lorimier P, et al. TUNEL apoptotic cell detection in tissue sections: Critical evaluation and improvement. J Histochem Cytochem 1998;46:327–34
69. de Torres C, Munell F, Ferrer I, et al. Identification of necrotic cell death by the TUNEL assay in the hypoxic-ischemic neonatal rat brain. Neurosci Lett 1997;230:1–4
70. Petito CK, Roberts B. Effect of postmortem interval on in situ end-labeling of DNA oligonucleosomes. J Neuropathol Exp Neurol 1995; 54:761–5

71. Kingsbury AE, Mardsen CD, Foster OJ. DNA fragmentation in human substantia nigra: Apoptosis or perimortem effect? Mov Disord 1998;13: 877–84

72. Torres G, Leheste JR, Ramos RL. Immunocytochemical localization of DNA double-strand breaks in human and rat brains. Neuroscience 2015;290:196–203

73. Yu SW, Wang H, Poitras MF, et al. Mediation of poly(ADP-ribose) polymerase-1-dependent cell death by apoptosis-inducing factor. Science 2002;297:259–63

74. Ame JC, Spenlehauer C, de Murcia G. The PARP superfamily. BioEssays 2004;26:882–93

75. Benit P, Goncalves S, Dassa EP, et al. The variability of the harlequin mouse phenotype resembles that of human mitochondrial-complex I-deficiency syndromes. PLoS One 2008;3:e3208

76. Coimbra-Costa D, Alva N, Duran M, et al. Oxidative stress and apoptosis after acute respiratory hypoxia and reoxygenation in rat brain. Redox Biol 2017;12:216–25

77. Novak CM, Ozen M, Burd I. Perinatal brain injury: Mechanisms, prevention, and outcomes. Clin Perinatol 2018;45:357–75

78. Ugwumadu A. Infection and fetal neurologic injury. Curr Opin Obstet Gynecol 2006;18:106–11

79. Zhao J, Chen Y, Xu Y, et al. Effect of intrauterine infection on brain development and injury. Int J Dev Neurosci 2013;31:543–9

80. Cande C, Cecconi F, Dessen P, et al. Apoptosis-inducing factor (AIF): Key to the conserved caspase-independent pathways of cell death? J Cell Sci 2002;115:4727–34

81. Klein JP, Waxman SG. The brain in diabetes: Molecular changes in neurons and their implications for end-organ damage. Lancet Neurol 2003;2:548–54

82. Culmsee C, Zhu C, Landshamer S, et al. Apoptosis-inducing factor triggered by poly(ADP-ribose) polymerase and Bid mediates neuronal cell death after oxygen-glucose deprivation and focal cerebral ischemia. J Neurosci 2005;25:10262–72

83. Slemmer JE, Zhu C, Landshamer S, et al. Causal role of apoptosis-inducing factor for neuronal cell death following traumatic brain injury. Am J Pathol 2008;173:1795–805

84. Thal SE, Zhu C, Thal SC, et al. Role of apoptosis inducing factor (AIF) for hippocampal neuronal cell death following global cerebral ischemia in mice. Neurosci Lett 2011;499:1–3

85. Burguillos MA, Hajji N, Englund E, et al. Apoptosis-inducing factor mediates dopaminergic cell death in response to LPS-induced inflammatory stimulus: Evidence in Parkinson's disease patients. Neurobiol Dis 2011;41:177–88

86. Czapski GA, Cakala M, Chalimoniuk M, et al. Role of nitric oxide in the brain during lipopolysaccharide-evoked systemic inflammation. J Neurosci Res 2007;85:1694–703

87. Peneder TM, Bauer J, Pifl C. Apoptosis-inducing factor in nigral dopamine neurons: Higher levels in primates than in mice. Mov Disord 2016;31:1729–33

88. Zhu C, Wang X, Huang Z, et al. Apoptosis-inducing factor is a major contributor to neuronal loss induced by neonatal cerebral hypoxia-ischemia. Cell Death Differ 2007;14:775–84

89. Zhang YF, Wang XY, Cao L, et al. Effects of hypoxic-ischemic brain injury on striatal dopamine transporter in newborn piglets: Evaluation of 11C-CFT PET/CT for DAT quantification. Nucl Med Biol 2011;38: 1205–12

90. Zhu C, Qiu L, Wang X, et al. Involvement of apoptosis-inducing factor in neuronal death after hypoxia-ischemia in the neonatal rat brain. J Neurochem 2004;86:306–17

91. Plesnila N, Zhu C, Culmsee C, et al. Nuclear translocation of apoptosis-inducing factor after focal cerebral ischemia. J Cereb Blood Flow Metab 2004;24:458–66

92. Xu Y, Wang J, Song X, et al. RIP3 induces ischemic neuronal DNA degradation and programmed necrosis in rat via AIF. Sci Rep 2016;6: 29362

93. Susin SA, Lorenzo HK, Zamzami N, et al. Molecular characterization of mitochondrial apoptosis-inducing factor. Nature 1999;397:441–6

94. Daugas E, Susin SA, Zamzami N, et al. Mitochondrio-nuclear translocation of AIF in apoptosis and necrosis. FASEB J 2000;14: 729–39

95. Bano D, Dinsdale D, Cabrera-Socorro A, et al. Alteration of the nuclear pore complex in Ca(2+)-mediated cell death. Cell Death Differ 2010; 17:119–33

96. Leist M, Single B, Castoldi AF, et al. Intracellular adenosine triphosphate (ATP) concentration: A switch in the decision between apoptosis and necrosis. J Exp Med 1997;185:1481–6

97. Lim ML, Mercer LD, Nagley P, et al. Rotenone and MPP+ preferentially redistribute apoptosis-inducing factor in apoptotic dopamine neurons. NeuroReport 2007;18:307–12

98. Kim TW, Moon Y, Kim K, et al. Dissociation of progressive dopaminergic neuronal death and behavioral impairments by Bax deletion in a mouse model of Parkinson's diseases. PLoS One 2011;6:e25346

99. Wang H, Shimoji M, Yu SW, et al. Apoptosis inducing factor and PARP-mediated injury in the MPTP mouse model of Parkinson's disease. Ann N Y Acad Sci 2006;991:132–9

100. Horn A, Adamcyzk C. Reticular formation: Eye movements, gaze and blinks. In: Mai J, Paxinos G, eds. *The Human Nervous System*. 3rd ed. Waltham, MA: Academic Press 2012:338–9

101. Ruzafa N, Rey-Santano C, Mielgo V, et al. Effect of hypoxia on the retina and superior colliculus of neonatal pigs. PLoS One 2017;12: e0175301

102. Horn AK, Eberhorn A, Hartig W, et al. Perioculomotor cell groups in monkey and man defined by their histochemical and functional properties: Reappraisal of the Edinger-Westphal nucleus. J Comp Neurol 2008;507:1317–35

103. Bergeron C, Petrunka C, Weyer L. Copper/zinc superoxide dismutase expression in the human central nervous system. Correlation with selective neuronal vulnerability. Am J Pathol 1996;148:273–9

104. Zhang J, Ma G, Guo Z, et al. Study on the apoptosis mediated by apoptosis-inducing-factor and influencing factors of bovine muscle during postmortem aging. Food Chem 2018;266:359–67

105. Pearson A. The oculomotor nucleus in the human fetus. J Comp Neurol 1944;80:47–63

106. Yamaguchi K. Development of the human oculomotor nuclear complex: Somatic nuclei. Ann Anat 2014;196:394–401

107. Roland EH, Jan JE, Hill A, et al. Cortical visual impairment following birth asphyxia. Pediatr Neurol 1986;2:133–7

108. Salati R, Borgatti R, Giammari G, et al. Oculomotor dysfunction in cerebral visual impairment following perinatal hypoxia. Dev Med Child Neurol 2007;44:542–50

109. Tastanbekov BD. Neurologic symptoms and syndromes in the diagnosis of perinatal brain lesions in newborn children. Zh Nevropatol Psikhiatr Im S S Korsakova 1979;79:1350–2

110. MacAskill MR, Anderson TJ. Eye movements in neurodegenerative diseases. Curr Opin Neurol 2016;29:61–8

111. Bittencourt J, Velasques B, Teixeira S, et al. Saccadic eye movement applications for psychiatric disorders. Neuropsychiatr Dis Treat 2013;9: 1393–409